Acta Crystallographica Section D
Biological Crystallography
ISSN 0907-4449

Structures of human deoxycytidine kinase product complexes

Erika V. Soriano, Valerie C. Clark and Steven E. Ealick*

Department of Chemistry and Chemical Biology, Cornell University, Ithaca, NY 14853-1301, USA

Correspondence e-mail: see3@cornell.edu

Received 18 July 2007
Accepted 4 October 2007

PDB References: dCK, dCMP/UDP/Mg^{2+} complex, 2qrn; dAMP/UDP/Mg^{2+} complex, 2qro.

Human deoxycytidine kinase (dCK) is involved in the nucleotide-biosynthesis salvage pathway and has also been shown to phosphorylate several antitumor and antiviral prodrugs. The structures of dCK alone and the dead-end complex of dCK with substrate nucleoside and product ADP or UDP have previously been reported; however, there is currently no structure available for a substrate or product complex. Here, the structures of dCK complexes with the products dCMP, UDP and Mg^{2+} ion, and with dAMP, UDP and Mg^{2+} ion are reported. Structural comparisons show that the product complexes with UDP and a dead-end complex with substrate and UDP have similar active-site conformations.

1. Introduction

Human deoxycytidine kinase (dCK; EC 2.7.1.74) catalyzes the phosphorylation of deoxycytidine (dC), deoxyadenosine (dA) or deoxyguanosine to the corresponding nucleotide monophosphate in the purine- and pyrimidine-salvage pathways using a nucleoside triphosphate as the phosphate donor. In addition to phosphorylating deoxynucleosides, dCK is the main activator of many nucleoside-analog prodrugs, including cladribine (2-chloro-2′-deoxyadenosine; Spasokoukotskaja *et al.*, 1995), AraC (1-β-D-arabinofuranosylcytosine; Kierdaszuk *et al.*, 1998), zalcitabine (2′,3′-dideoxycytidine; Johnson *et al.*, 1987) and lamivudine (2′-deoxy-3′-thiacytidine; Kewn *et al.*, 1997). Phosphorylation of the monophosphate is the rate-limiting step in prodrug activation and prevents the nucleotide from diffusing out of the cell. Drug resistance to many nucleoside analogs has been linked to dCK activity (Groschel *et al.*, 1999; Mansson *et al.*, 1999; Stegmann *et al.*, 1995). Biochemical characterizations have shown that dCK has a turnover rate below 1 s^{-1} *in vitro* and is much slower than other nucleoside kinases such as deoxyguanosine kinase (dGK; Hughes *et al.*, 1997; Johansson *et al.*, 1999); therefore, understanding the active site of dCK and its substrate requirements is an important consideration in the design of novel nucleoside analogs with chemotherapeutic potential.

Early studies have also shown that in addition to its broad substrate specificity, dCK can utilize a wide variety of nucleotide triphosphate donors including uridine triphosphate (UTP), adenosine triphosphate (ATP) and guanosine triphosphate (GTP). Kinetics studies have shown that UTP is the preferred phosphate donor over ATP and GTP, although ATP is found in larger quantities in the cell (Shewach *et al.*, 1992; White & Capizzi, 1991). Recent *in vivo* studies have revealed that dCK activity is modulated by phosphorylation of Ser74

Table 1
Data-collection and refinement statistics.

Values in parentheses are for the highest resolution bin.

	dCMP/UDP/Mg^{2+}	dAMP/UDP/Mg^{2+}
Data collection		
Beamline	CHESS A1	APS 24-ID-C
Wavelength (Å)	0.9764	0.9795
Resolution (Å)	3.4 (3.52–3.40)	3.45 (3.57–3.45)
Space group	$P4_32_12$	$P4_32_12$
Unit-cell parameters		
$a = b$ (Å)	94.5	93.7
c (Å)	335.3	332.4
No. of reflections	113065	152111
No. of unique reflections	21038	18290
Redundancy	5.4 (3.2)	8.3 (8.4)
Completeness (%)	95.4 (73.3)	89.1 (89.0)
R_{sym}† (%)	12.9 (38.9)	10.5 (44.6)
$I/\sigma(I)$	10.2 (2.5)	13.6 (3.2)
Refinement		
Total No. of non-H atoms	7704	7816
No. of protein atoms	7520	7520
No. of ligand atoms	184	296
R factor‡ (%)	22.7	19.8
R_{free}§ (%)	28.1	25.8
R.m.s. deviation from ideal geometry		
Bonds (Å)	0.01	0.008
Angles (°)	1.2	1.2
B factors (Å^2)		
Protein	60.8	55.1
Ligands	56.4	48.2
Ramachandran plot		
Most favored region (%)	81.2	80.3
Additionally allowed region (%)	18.3	18.5
Generously allowed region (%)	0.0	0.7
Disallowed region (%)	0.5	0.5

† $R_{sym} = \sum\sum_i |I_i - \langle I\rangle| / \sum\langle I\rangle$, where $\langle I\rangle$ is the mean intensity of the N reflections with intensity I_i and common indices hkl. ‡ R factor $= \sum_{hkl} ||F_{obs}| - k|F_{calc}|| / \sum_{hkl} |F_{obs}|$, where F_{obs} and F_{calc} are observed and calculated structure factors, respectively. § For R_{free}, the sum is extended over a subset of reflections (5%) that were excluded from all stages of refinement.

(Smal *et al.*, 2006); therefore, the actual kinetic rates *in vivo* may be faster than those reported *in vitro*.

Several crystal structures of ternary dCK complexes have been reported. These dead-end complexes include those with dC/adenosine diphosphate (ADP) (Sabini *et al.*, 2003), AraC/ADP/Mg^{2+} (Sabini *et al.*, 2003), gemcitabine/ADP/Mg^{2+} (Sabini *et al.*, 2003), (−)-β-2′,3′-dideoxy-3′-thiacytidine/ADP (Sabini *et al.*, 2007), troxacitabine/ADP (Sabini *et al.*, 2007), clofarabine/ADP (Zhang *et al.*, 2006) and dC/uridine diphosphate (UDP)/Mg^{2+} (Godsey *et al.*, 2006). All of the dead-end complexes contain a nucleoside-analog substrate and the product ADP, with the exception of the dC/UDP/Mg^{2+} structure (Godsey *et al.*, 2006). This structure was obtained from a mutant that lacked a flexible-loop region (residues 65–79). Crystallization with UDP revealed a main-chain rearrangement that was not seen in the ADP complexes, explaining the preference for UTP over ATP as the phosphate donor. Here, we report the structures of two product complexes with the full-length enzyme. The first product complex contains dCMP (deoxycytidine monophosphate), UDP and Mg^{2+} ion, while the second complex contains dAMP (deoxyadenosine monophosphate), UDP and Mg^{2+} ion. The main-chain rearrangement seen in the dC/UDP/Mg^{2+} complex is also seen in these product complexes.

2. Experimental procedures

2.1. Protein expression and purification

The human dCK gene was cloned into the plasmid pDCK.28 as described previously (Zhang *et al.*, 2006). The pDCK.28 plasmid was transformed into *Escherichia coli* BL21(DE3) cells (Novagen). Starter cultures of the transformed cells were grown overnight at 310 K in 10 ml LB media with 50 µg ml^{-1} kanamycin. The culture was divided into two 1 l flasks containing 2YT media and shaken at 200 rev min^{-1} at 310 K until the OD_{600} reached ∼0.8, at which point 0.1 m*M* isopropyl β-D-1-thiogalactopyranoside was added to induce protein expression. The cells were induced for 6 h and then spun down at 6500*g* for 15 min.

All dCK purification steps were carried out at 277 K. The cells were resuspended in 40 ml lysis buffer (10 m*M* imidazole, 50 m*M* Na_2HPO_4, 300 m*M* NaCl pH 7.0) containing 0.1 mg ml^{-1} lysozyme and lysed by sonication. The crude extract was centrifuged at 27 000*g* for 30 min and the supernatant was loaded onto an Ni–NTA resin (Novagen) column pre-equilibrated with lysis buffer. The protein was washed with 150 ml lysis buffer and eluted with buffer containing 300 m*M* imidazole, 50 m*M* Na_2HPO_4, 300 m*M* NaCl pH 7.0. The protein was buffer-exchanged into 20 m*M* HEPES, 10 m*M* $MgCl_2$, 5 m*M* dithiothreitol at pH 7.0 using an Econo-Pac 10DG (Bio-Rad) and then concentrated to 13 mg ml^{-1} using an Amicron Ultra-15 centrifugal filter device. The protein was found to be >95% pure by Coomassie-stained SDS–PAGE (data not shown).

2.2. dCK crystallization

The dCK complexes were crystallized at 295 K using the hanging-drop vapor-diffusion method. All crystallization drops consisted of 1 µl protein solution and 1 µl well solution. The protein solution contained dCK at a concentration of 13 mg ml^{-1}, 2 m*M* of the phosphate donor UTP and 2 m*M* substrate (either dC or dA). For the dC/UTP/Mg^{2+} complex, the well solution was optimized to contain 16–17% ethanol, 0.1 *M* HEPES pH 7.0–7.1. The cryoprotectant consisted of the mother liquor with 30% ethylene glycol. For the dA/UTP/Mg^{2+} complex, the well solution was optimized to 16–17% ethanol, 0.1 *M* HEPES pH 7.0–7.1, 8% glycerol. The cryoprotectant contained 20% ethanol, 0.1 *M* HEPES pH 7.0 and 20% glycerol.

The crystals grew as needle clusters overnight to maximum dimensions of 0.06 × 0.06 × 0.4 mm. The crystals were briefly transferred into the cryoprotectant, flash-frozen by plunging into liquid nitrogen and stored for later use. Initial X-ray data showed that both the dC/UTP/Mg^{2+} and the dA/UTP/Mg^{2+} crystals belong to space group $P4_32_12$, with the dC/UTP/Mg^{2+} complex having unit-cell parameters a = 94.5, c = 335.3 Å and the dA/UTP/Mg^{2+} crystals having unit-cell parameters a = 93.7, c = 332.4 Å. The crystals contained two dimers of dCK per

asymmetric unit, corresponding to a solvent content of 60% and a Matthews number of 3.0 Å^3 Da^{-1} (Matthews, 1968).

2.3. Data collection and processing

Data for the dC/UTP/Mg^{2+} crystals were collected at the Cornell High Energy Synchrotron Source (CHESS) beamline A1 using a Quantum 210 detector (Area Detector Systems Corporation) in unbinned mode. The data were collected with an oscillation of 0.5° at a wavelength of 0.9764 Å. The data for the dA/UTP/Mg^{2+} crystals were collected at the Advanced Photon Source (APS) beamline 24-ID-C using a Quantum 315 detector (Area Detector Systems Corporation) in binned mode. The data were collected at a wavelength of 0.9795 Å with an oscillation of 1.0°. The *HKL*-2000 suite (Otwinowski & Minor, 1997) was used to index, integrate and scale both data sets. Table 1 summarizes the final data-collection and processing statistics.

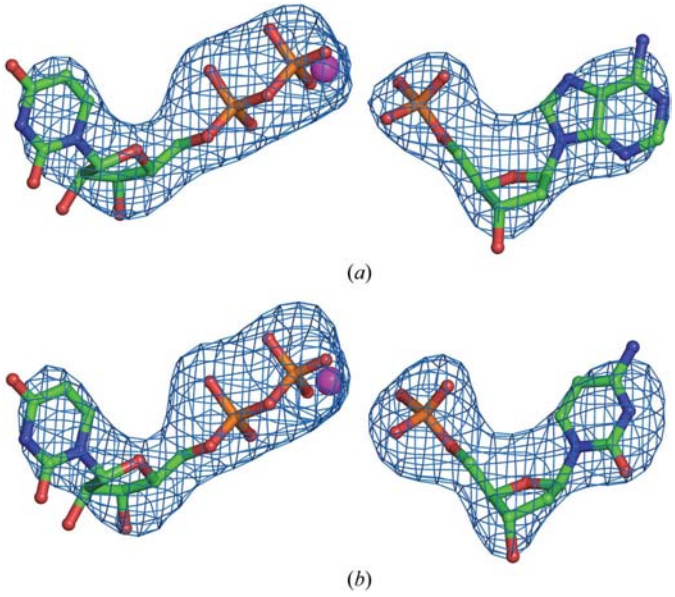

Figure 1
Difference electron density for the products. (*a*) MgUDP and dAMP. (*b*) MgUDP and dCMP. The difference electron density was calculated using model phases with the ligand atoms removed. The maps are averaged using fourfold NCS and contoured at 3σ.

2.4. Structure determination and model refinement

The structures of the dCK complexes were solved by molecular replacement using *CNS* (Brünger *et al.*, 1998) with the human dCK structure (PDB code 1p60) as the search model. Model building was performed using the programs *O* (Jones *et al.*, 1991) and *Coot* (Emsley & Cowtan, 2004). Noncrystallographic symmetry (NCS) averaged electron-density maps (*RAVE*; Kleywegt & Jones, 1997, 1999) were used for model building and refinement. Several rounds of refinement were performed in *CNS* using tight NCS restraints for the main chain and medium-tight restraints for the side chains. The active-site electron density clearly showed the presence of the products dCMP/UDP/Mg^{2+} or dAMP/UDP/Mg^{2+} in the crystals grown in dC/UTP/Mg^{2+} and dA/UTP/Mg^{2+}, respectively; therefore, the products dCMP/UDP/Mg^{2+} and dAMP/UDP/Mg^{2+} were built into each active site (Fig. 1). Final refinement statistics are shown in Table 1.

3. Results

3.1. Overall structure

The structures of human dCK complexed with dCMP/UDP/Mg^{2+} and dAMP/UDP/Mg^{2+} were determined to 3.40 and 3.45 Å resolution, respectively. The final model contains two dimers in the asymmetric unit. Residues 1–19 and 64–76 were disordered in all four protomers for both product complexes and were not included in the final model. Each protomer consists of a three-layer $\alpha/\beta/\alpha$ sandwich (Fig. 2) as previously described (Zhang *et al.*, 2006), with a five-stranded parallel β-sheet flanked by ten α-helices. The four protomers in the asymmetric unit are arranged as a pair of dimers, with α4 and α7 forming a four-helix bundle at the dimer interface. A Ramachandran plot revealed that Arg128, an active-site residue with good electron density, is in the disallowed region for all four protomers in both product complexes. This residue is also in the disallowed region for other dCK structures deposited in the Protein Data Bank.

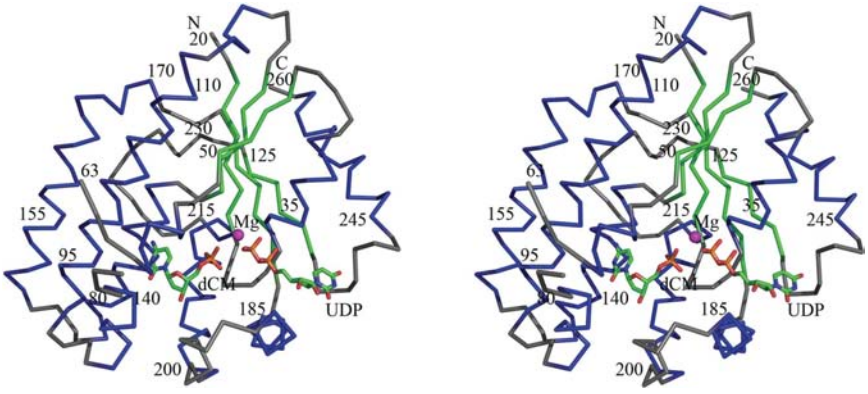

Figure 2
Stereoview of the C^{α} trace of wild-type human dCK complex, with α-helices shown in blue and β-strands shown in green. The products dCMP and UDP are shown in stick representation and are colored by atom, with green for carbon, blue for nitrogen, red for oxygen and orange for phosphorus. The magnesium ion is shown as a magenta sphere.

3.2. Deoxynucleoside-binding site

The product mononucleotides are bound to the active site through extensive hydrogen bonds. The pyrimidine N3 atom forms a hydrogen bond to the amide group of Gln97, while the N4 atom forms a hydrogen bond to the carboxylate side chain of Asp133. The 3′ sugar hydroxyl forms a hydrogen bond with the Tyr86 and Glu197 side chains. The phosphate O1 atom interacts with Arg128 and the O3 atom forms a

hydrogen bond to Arg192. In the dAMP/UDP/Mg^{2+} complex, the purine N1 atom forms a hydrogen bond to the amide group of Gln97. The N6 amino group interacts with Asp133, while the N7 atom forms a hydrogen bond to the Glu53 side chain. The sugar hydroxyl forms hydrogen bonds to Tyr86 and Glu197 similarly to the dCMP ligand. The phosphate O1 atom forms a hydrogen bond to Arg128. The O3 atom also forms a hydrogen bond to Arg192, with the arginine side chain closer to the O3 atom in the dAMP complex compared with the dCMP complex (Fig. 3).

Several hydrophobic interactions also contribute to product binding. In the dCMP/UDP/Mg^{2+} structure, the pyrimidine ring of dCMP is involved in parallel stacking interactions with Phe137. Phe137 is part of a hydrophobic pocket which includes Phe96, which is ~3.7 Å away from the pyrimidine ring, and Trp58, which is ~3.9 Å away from the pyrimidine ring. In the dAMP/UDP/Mg^{2+} product complex, the purine ring of dAMP also forms parallel stacking interactions with Phe137 and hydrophobic interactions with Phe96 and Trp58, which are both ~3.8 Å away from the purine ring.

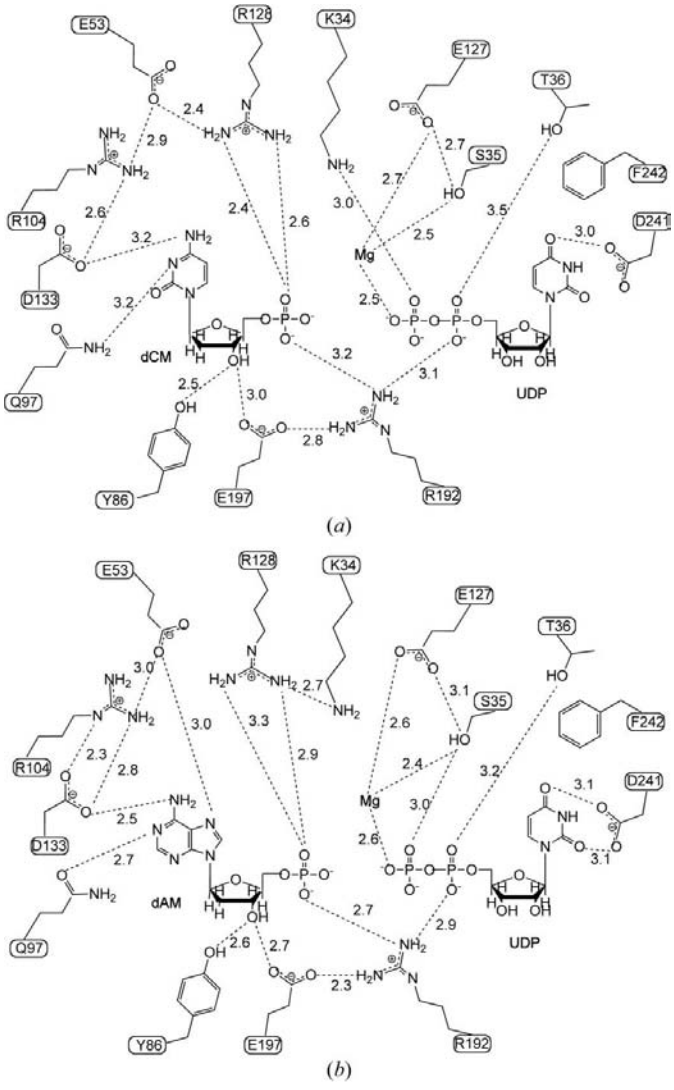

Figure 3
Schematic representation of the active site. (*a*) The dCMP/UDP/Mg^{2+} complex. (*b*) The dAMP/UDP/Mg^{2+} complex.

3.3. UDP-binding site

The UDP hydrogen-bonding patterns are similar for both complexes. The UDP β-phosphate group forms electrostatic interactions with the Mg^{2+} ion. The α-phosphate group also interacts with the Arg192 and Thr36 side chains in both complexes; however, the UDP moiety has been shifted in the active site by approximately 0.5 Å to make room for the adenosine ring in the dAMP/UDP/Mg^{2+} complex. This shift results in the pyrimidine ring of UDP forming two hydrogen bonds to the Asp241 side chain instead of the single hydrogen bond observed in the dCMP/UDP/Mg^{2+} complex. In the dAMP/UDP/Mg^{2+} complex the β-phosphate of UDP forms a hydrogen bond to the side chain of Ser35; however, in the dCMP/UDP/Mg^{2+} complex the β-phosphate interacts with Lys34 (see Fig. 3). The UDP-binding site is fairly solvent-exposed; however, there are a few hydrophobic interactions near the pyrimidine ring that are present in both product complexes. The pyrimidine ring is ~3.9 Å away from the Phe242 side chain, which is part of a hydrophobic pocket in the interior of the UDP-binding site. Above the pyrimidine ring, Arg188 is found in an extended conformation ~4.2 Å away.

4. Discussion

4.1. Quality of the dCK product-complex structures

The structures of the two product complexes reported here were determined at modest resolution (3.4–3.45 Å). However, the asymmetric unit contains four protomers and NCS averaging compensates in part for the effects of low resolution. Many of the dCK structures to which we compare the product complexes were determined at much higher resolution (as high as 1.7 Å) and the reader should take this into account in assessing the significance of the similarities and differences.

4.2. Comparisons of the dCMP/UDP/Mg^{2+} and dAMP/UDP/Mg^{2+} complexes

Comparison of the active sites in the dCMP/UDP/Mg^{2+} and dAMP/UDP/Mg^{2+} complexes shows that the UDP-ligand position differs by about 0.5 Å. The shift results in the formation of two hydrogen bonds to the Asp241 side chain and makes room for the larger purine base of dAMP (Fig. 4*a*). The shift in the UDP results in a loss of a hydrogen bond to Lys34 and the formation of a new hydrogen bond between Ser35 and the β-phosphate. Therefore, the shift in the UDP ligand in the active site results in no net gain or loss in the number of hydrogen bonds. The hydrogen-bonding pattern is also altered near the pyrimidine/purine-ring binding site of dCMP and dAMP (Fig. 4*a*). The r.m.s.d. between the dCMP complex and the dAMP complex based on the C^{α} positions of residues 20–63 and 77–165 is 0.4 Å; however, the resolution of the product complexes prevents a detailed comparison.

4.3. Comparison of the dCMP/UDP/Mg^{2+} and dC/UDP/Mg^{2+} structures

The structure of the dC/UDP/Mg^{2+} complex (PDB code 2a2z) was previously solved using a dCK mutant that lacks residues 65–79 (Godsey *et al.*, 2006). A comparison of the active sites of the dC/UDP/Mg^{2+} and dCMP/UDP/Mg^{2+} complexes shows small differences in the UDP binding site and the dCMP-binding site (Fig. 4*b*). The largest difference between these two structures is at the position of the Mg^{2+} ion. A superposition of the two structures reveals a difference in Mg^{2+}-ion position of about 1.5 Å. Also visible from the superposition is the movement of residues 241–246. These residues are located near the UDP binding site, with residues Asp241 and Phe242 interacting with the pyrimidine ring of UDP. Residues Asp241 and Phe242 are in a different rotameric conformation in the dCMP/UDP/Mg^{2+} structure compared with the dC/UDP/Mg^{2+} structure. The main-chain atoms have also been shifted, especially near Asn244, where the C^{α} atom is shifted ∼2.7 Å. The overall r.m.s.d. between the two complexes is 0.7 Å based on the C^{α} positions of residues 20–63 and 77–165.

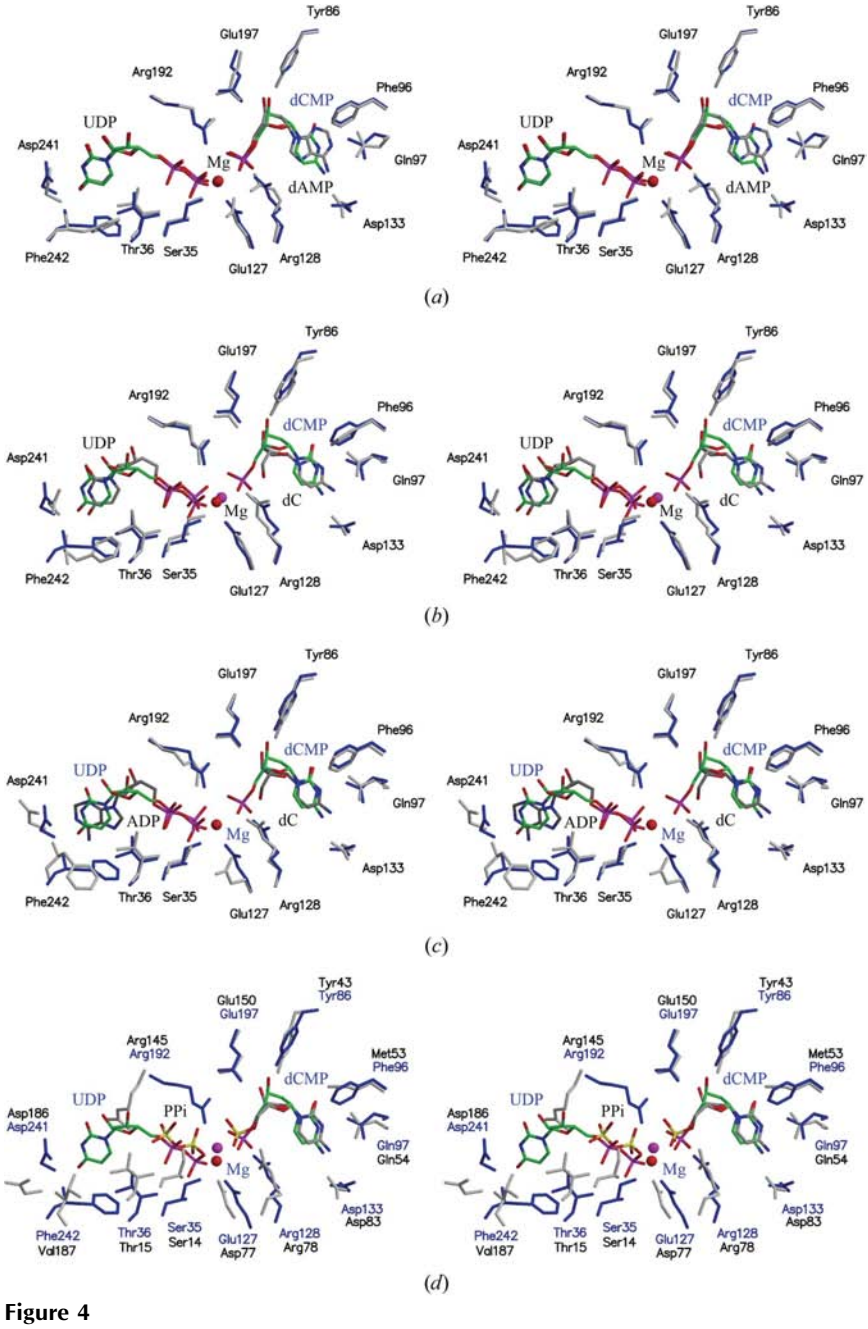

Figure 4
Active-site superposition of human dCK complexes. (*a*) Superposition of the dCMP/UDP/Mg^{2+} complex with the dAMP/UDP/Mg^{2+} complex. (*b*) Superposition of the dCMP/UDP/Mg^{2+} complex with the dC/UDP/Mg^{2+} complex. (*c*) Superposition of the dCMP/UDP/Mg^{2+} complex with the dC/ADP complex. (*d*) Superposition of the human dCK dCMP/UDP/Mg^{2+} and dAK complexes. The dCK side chains and numbering are shown in blue, while the dAK active-site side chains and numbering are shown in gray and black, respectively. The ligands PP_i and dCMP are shown in stick representation, with carbon colored gray, nitrogen blue, oxygen red and phosphorus yellow. The dCMP/UDP/Mg^{2+} complex is shown in blue in all cases, with the ligands shown in stick representation with carbon colored green, nitrogen blue, oxygen red and phosphorus magenta; Mg^{2+} is shown as a red sphere. In (*a*)–(*c*), the other dCK complexes are shown in gray, with the ligands shown in stick representation with carbon colored gray, nitrogen blue, oxygen red and phosphorus magenta; Mg^{2+} is shown as a magenta sphere.

4.4. Comparison of the dCMP/UDP/Mg^{2+} and dC/ADP dCK structures

The structure of dCK bound to dC/ADP was compared with the product complex dCMP/UDP/Mg^{2+} and revealed no major conformational differences near the pyrimidine ring. There is a slight rotation of the dCMP with respect to dC resulting from an interaction between the phosphate group and Arg192 (Fig. 4*c*). The largest differences between the dCMP/UDP/Mg^{2+} complex and the dC/ADP complex occur at the UDP-binding site involving residues 241–247. In particular, Lys243 has shifted 3.4 Å closer to the pyrimidine ring in the dCMP/UDP/Mg^{2+} structure. This main-chain rearrangement is also seen in the previously published dC/UDP/Mg^{2+} mutant complex (Godsey *et al.*, 2006). These conformational changes are also present in dAMP/UDP/Mg^{2+} product complexes.

4.5. dCK/dAK active-site comparisons

Human Dgk, *Drosophilia melanogaster* dNK and dCK share a common fold (Johansson *et al.*, 2001). Recently, the structure of deoxyadenosine kinase (dAK) from *Mycoplasma mycoides* (PDB code 2jat) was reported (Welin *et al.*, 2007) and shown to be a member of this kinase superfamily. Kinetic studies showed that dA is the preferred substrate of dAK, although like dCK it also exhibits wide substrate

specificity (Wang *et al.*, 2001). The dAK complex with dCMP, deoxycytidine diphosphate (dCDP) and Mg^{2+} at 2.6 Å resolution (PDB code 2jat) showed weak density for dCDP and only the pyrophosphate (PP_i) was included in the model. A superposition of dCK with dAK revealed similar dCMP-binding sites (Fig. 4*d*). All the residues involved in dCMP binding are conserved, with the exception of Phe96, which is Met53 in dAK; however, the UDP-binding site of dCK does not superimpose well with dAK. Although most of the residues involved in UDP binding in dCK are structurally conserved in dAK, the residues adopt different rotomeric conformations. The most striking difference can be seen in Arg192. In the dCK structure Arg192 is facing in the opposite direction to the corresponding arginine residue in the dAK structure. The differences may be a consequence of the low occupancy of the dCDP in the dAK structure as well its preference for ATP instead of UTP as the phosphate donor.

4.6. dCK phosphorylation

The dC/UDP/Mg^{2+} complex (PDB code 2a2z) was previously reported using a dCK mutant that lacks residues 65–79 (Godsey *et al.*, 2006). These residues correspond to an insertion that is present in dCK but not in the related dGK and nucleoside kinase (dNK) structures. Although full-length protein was used for crystallization, residues 63–76 were disordered in the dCMP/UDP/Mg^{2+} complex structure. Previous studies showed that dCK is regulated *in vivo* by phosphorylation (Smal *et al.*, 2006). Although dCK has several potential phosphorylation sites, the primary site of phosphorylation is at residue Ser74. It has also been shown that phosphorylation of Ser74 results in an increased activity over the nonphosphorylated form (Smal *et al.*, 2006). Ser74 is located on a flexible loop that is usually disordered in the dCK structures. However, a dC/ADP complex of dCK in space group $C222_1$ contained one monomer with an ordered loop (Sabini *et al.*, 2003). Superpositions of the dCMP/UDP/Mg^{2+} complex with the dC/ADP complex show Ser74 to be approximately 30 Å away from the active site and 35 Å away from the active site of the adjacent protomer (Fig. 5). The observed loop conformation may be influenced by crystal-packing interactions and when Ser74 is phosphorylated the loop might form a lid over the active site.

5. Conclusion

dCK is often the rate-limiting step in the activation of nucleoside-analog prodrugs. Structural studies provide insight into the active-site geometry, the details of substrate specificity and the mechanism by which dCK activates prodrugs. The product complexes of dCK reveal additional areas of structural flexibility and how the dCK active site can accommodate a variety of substrates. However, questions remain concerning the active form of dCK *in vivo*. In particular, how does the phosphorylation increase the activity of the enzyme and by what mechanism? Structures of dCK complexes with a phosphorylated Ser74 will be needed to further understand the activity of the enzyme *in vivo* and to provide additional details for nucleoside-analog design.

We would like to acknowledge CHESS A1, supported by NIH grant RR-01646, and the Northeastern Collaborative Access Team beamline 24-ID-C of the Advanced Photon Source, supported by award grant RR-15301 from the National Center for Research Resources at the National Institutes of Health. Use of the Advanced Photon Source is supported by the US Department of Energy, Office of Basic Energy Sciences under Contract No. DE-AC02-06CH11357. The authors would also like to acknowledge Ms Leslie Kinsland for assistance in preparing this manuscript and Dr Cynthia Kinsland for preparing the dCK over-expression plasmid.

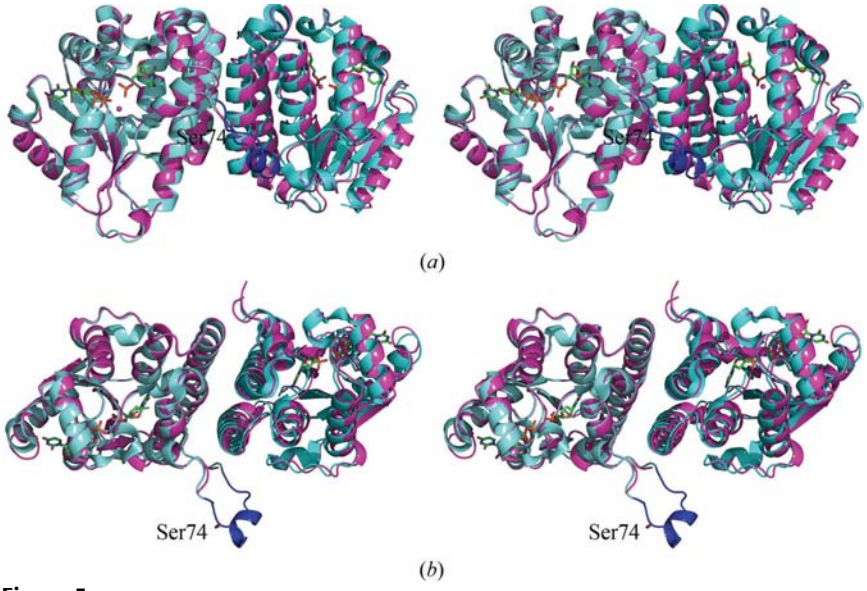

Figure 5
dCK UDP/dCMP/Mg^{2+} complex (magenta) superimposed on the dCK dC/ADP complex (cyan). (*a*) Side view, (*b*) top view. UDP and dCMP ligands are shown in stick representation with carbon green, oxygen red, nitrogen blue and phosphorous orange; Mg^{2+} ions are shown as magenta spheres. Residues 65–79 are colored blue, with Ser74 from the dC/ADP complex shown in stick representation.

References

Brünger, A. T., Adams, P. D., Clore, G. M., DeLano, W. L., Gros, P., Grosse-Kunstleve, R. W., Jiang, J.-S., Kuszewski, J., Nilges, M., Pannu, N. S., Read, R. J., Rice, L. M., Simonson, T. & Warren, G. L. (1998). *Acta Cryst.* D**54**, 905–921.
Emsley, P. & Cowtan, K. (2004). *Acta Cryst.* D**60**, 2126–2132.
Godsey, M. H., Ort, S., Sabini, E., Konrad, M. & Lavie, A. (2006). *Biochemistry*, **45**, 452–461.
Groschel, B., Himmel, N., Cinatl, J., Perigaud, C., Gosselin, G., Imbach, J. L., Doerr, H. W. &

Cinatl, J. Jr (1999). *Nucleosides Nucleotides*, **18**, 921–926.
Hughes, T. L., Hahn, T. M., Reynolds, K. K. & Shewach, D. S. (1997). *Biochemistry*, **36**, 7540–7547.
Johansson, K., Ramaswamy, S., Ljungcrantz, C., Knecht, W., Piskur, J., Munch-Petersen, B., Eriksson, S. & Eklund, H. (2001). *Nature Struct. Biol.* **8**, 616–620.
Johansson, M., van Rompay, A. R., Degreve, B., Balzarini, J. & Karlsson, A. (1999). *J. Biol. Chem.* **274**, 23814–23819.
Johnson, M. A., Johns, D. G. & Fridland, A. (1987). *Biochem. Biophys. Res. Commun.* **148**, 1252–1258.
Jones, T. A., Zou, J.-Y., Cowan, S. W. & Kjeldgaard, M. (1991). *Acta Cryst.* A**47**, 110–119.
Kewn, S., Veal, G. J., Hoggard, P. G., Barry, M. G. & Back, D. J. (1997). *Biochem. Pharmacol.* **54**, 589–595.
Kierdaszuk, B., Krawiec, K., Kazimierczuk, Z., Jacobsson, U., Johansson, N. G., Munch-Petersen, B., Eriksson, S. & Shugar, D. (1998). *Adv. Exp. Med. Biol.* **431**, 623–627.
Kleywegt, G. J. & Jones, T. A. (1997). *Acta Cryst.* D**53**, 179–185.
Kleywegt, G. J. & Jones, T. A. (1999). *Acta Cryst.* D**55**, 941–944.
Mansson, E., Spasokoukotskaja, T., Sallstrom, J., Eriksson, S. & Albertioni, F. (1999). *Cancer Res.* **59**, 5956–5963.
Matthews, B. W. (1968). *J. Mol. Biol.* **33**, 491–497.
Otwinowski, Z. & Minor, W. (1997). *Methods Enzymol.* **276**, 307–326.
Sabini, E., Hazra, S., Konrad, M., Burley, S. K. & Lavie, A. (2007). *Nucleic Acids Res.* **35**, 186–192.
Sabini, E., Ort, S., Monnerjahn, C., Konrad, M. & Lavie, A. (2003). *Nature Struct. Biol.* **10**, 513–519.
Shewach, D. S., Reynolds, K. K. & Hertel, L. (1992). *Mol. Pharmacol.* **42**, 518–524.
Smal, C., Vertommen, D., Bertrand, L., Ntamashimikiro, S., Rider, M. H., Van Den Neste, E. & Bontemps, F. (2006). *J. Biol. Chem.* **281**, 4887–4893.
Spasokoukotskaja, T., Arner, E. S., Brosjo, O., Gunven, P., Juliusson, G., Liliemark, J. & Eriksson, S. (1995). *Eur. J. Cancer*, **31**A, 202–208.
Stegmann, A. P., Honders, M. W., Hagemeijer, A., Hoebee, B., Willemze, R. & Landegent, J. E. (1995). *Ann. Hematol.* **71**, 41–47.
Wang, L., Westberg, J., Bolske, G. & Eriksson, S. (2001). *Mol. Microbiol.* **42**, 1065–1073.
Welin, M., Wang, L., Eriksson, S. & Eklund, H. (2007). *J. Mol. Biol.* **366**, 1615–1623.
White, J. C. & Capizzi, R. L. (1991). *Cancer Res.* **51**, 2559–65.
Zhang, Y., Secrist, J. A. & Ealick, S. E. (2006). *Acta Cryst.* D**62**, 133–139.